Peer-reviewed version available at Crystals 2018, 8, 421; doi:10.3390/cryst8110421

Optical Detection of Green Emission for Non-Uniformity Film in Flat Panel Display

Fu-Ming Tzu[1] and Jung-Hua Chou[2]

[1]Department of Marine Engineering, National Kaohsiung University of Science and Technology, Kaohsiung, Taiwan, fuming88@nkust.edu.tw

[2]Department of Engineering Science, National Cheng Kung University, Tainan, Taiwan, jungchou@mail.ncku.edu.tw

[1]Correspondence: fuming88@nkust.edu.tw, Tel: +886-7-810-0888 ext. 25245

Abstract

Among colours, the green has the most sensitivity in human vision so that green defects on displays can be effortlessly perceived by a photopic eye with the most intensity in the wavelength 555 nm of the spectrum. With the market moving forward to high resolution, displays can have resolutions of 10 million pixels. Therefore, the task detects the appearance the panel using ultra-high resolutions in TFT-LCD. The machine vision associated with reflective chromaticity spectrometer quantises the defects are explored, such as blackening and whitening. The result shows the significant phenomena to recognize the non-uniformity film-related chromatic tendency. In contrast, the quantitative assessment illuminates that the chromaticity CIE xyY at 0.001 is a just noticeable difference (JND) and detects even more sensitivity. Moreover, an optical device associated with a ^{198}Hg discharge lamp calibrates the spectrometer accuracy.

Keywords:

optical, green, colour difference, chromaticity, just noticeable difference.

Introduction

With the ultra-high resolution leading mainstream technology, the characteristics demonstrates a high imaging resolution, wider view, sharp contrast, quick response, very low power consumption, and minimum radiation[1, 2]. The wide-colour gamut and high-dynamic range using red, green, blue and white (RGBW) LCDs, the colour gamut reaches over 100% National Television Standards Committee (NTSC). Moreover, the RGBW LCDs enhance 50% higher light transmission [3]. Three common aspect ratios are compared diagonally as Figure 1. The widest blue frame (2.35:1) is the picture aspect ratio commonly used in movies. The green frame (16:9) and the red box near the square (4:3) are the standard ratios commonly used in television. The aspect ratio is the ratio of the width of an image divided by its height, is usually expressed as "X:Y" or "X^{x}Y", where the colon and the cross indicate the "ratio".

Currently, the most commonly used in the film industry is the anamorphic ratio at 2.39:1. The traditional 4:3 (1.33:1) is still used on today's analogy TV, and the specification of successful successor is at 16:9 (1.78:1) is used for high-definition TVs. These three ratios are the three standard ratios specified by the MPEG-2 (DVD) digital compression format, while 16:9 is also used by Blu-ray disc and HD DVD, and is also a compromise between the two commonly used 35 mm film. With the market continuing forward, the aspect ratio of the screen enlarges from 4:3 to 16:9 even more ration.

Recently, the technology of the flat panel display (FDP) has extended its view resolution from high definition (HD) to ultra-high definition (UHD) by 2 K (1920*1080) and 4 K (3840*2160). More display makers are developing 8 K (7680*4320), 16 K (15360*8640), and beyond 32 K (30720*17280). As 4 K is four times as many pixels as 2 K resolution, while 8 K also has four times the capacity of 4 K, and 16 K indicates four times pixels of 8 K, names this era of development ‘FPD 4 times’[4]. The content will be full high-resolution images to enrich the stereoscopic visibility of the pixels [5, 6]. The colour filter is the major optical component to present full colours comprising red, green, blue (RGB), and even yellow (Y). The photopic eye sensitivity has a maximum sensitivity in the green spectral range at 555 nm that green light is the most sensitive to human eyes [7]. Spot non-uniformity is a common defect caused by abnormal processing, which has an extremely low contrast display. The morphology is quite invisible so that human eyes hardly perceive any defects. The task treats this phenomenal invisibility as a criterion for the just noticeable difference (JND); which focuses on a perceptibility associated charge-couple device (CCD) with a chromaticity spectrometer to quantify the green emissive layer.

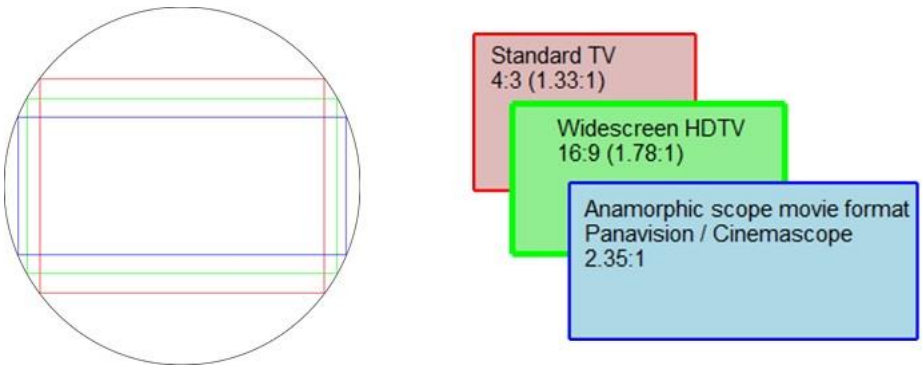

Figure 1 Three common aspect ratios are compared diagonally which, red near the square (4:3), green frame (16:9) and blue frame (2.35:1) in the flat panel display, accordingly.

Principle

The task utilises the line-scan CCD to detect non-uniformity defects on TFT-LCDs at one time, which is very efficient and effectively. The line-scan of time-delay-integration (TDI) of the charge couple device (CCD) on large generation's TFT-LCDs is very impressive. A commercial off-the-shelf TDI CCD, Dalsa Inc., a key component of the machine vison provides the fast responsivity compared to other line CCD. The TDI CCD of photo sensor offers the scanning mode under low light and slow speed during TDI mode. The photo sensor grabs an image of the moving object while transfers the charge, synchronous scanning with the object, i.e., the scanning image synchronization. In the scanning operating mode, the wavelengths of the light source include ultra-ultraviolet (UV), visual wavelengths, near infrared (NIR), and infrared (IR). Thus, this light source can reflect various responses to trigger the captured by line CCD. Currently, manual optical inspection (MOI) is used to observe the non-uniformity of colour filters by human eyes that identify diversified non-uniformity through various light sources, including fluorescent light, halide lamp, sodium lamp, and light-emitted diode (LED). However, its indication has a drawback, which is human subjective judgement. In contrast, human vision plays a major role in inspecting non-uniformity features in the display field. Thus, the machine vision as an automatic optical inspection (AOI) to support for MOI is very reliable in the task. The architecture is shown in Figure 2. The left of the figure is a MOI and the right of the figure is an AOI.

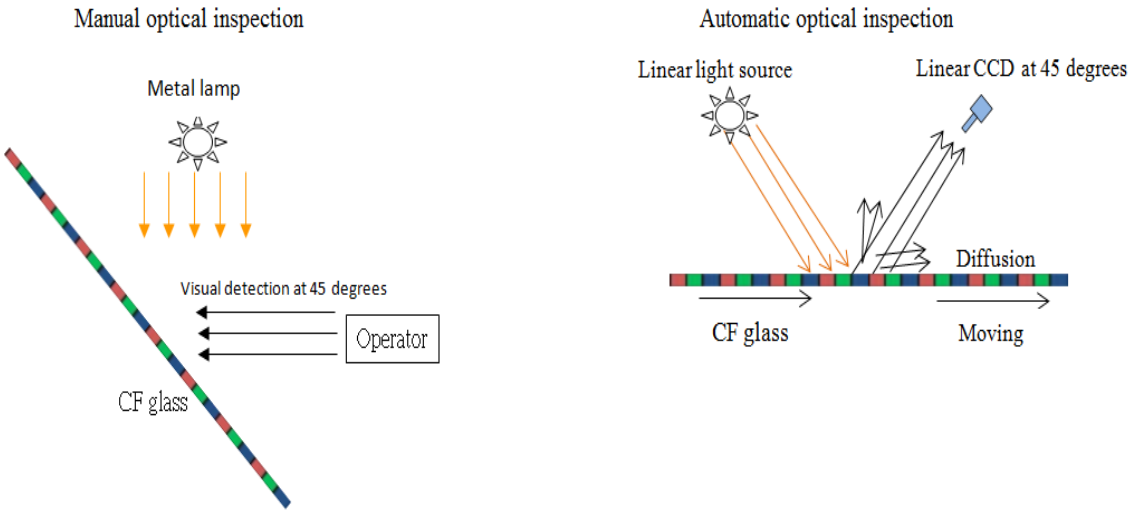

Figure 2 Architecture of optical inspection, MOI (left) vs AOI (right) [4, 8].

The characteristics of non-uniformity appears the trend for chromaticity or thickness so that typically inspects its appearance at the grey level variant. An edging detection method is used to compare the grad level of the threshold between the background and the selected area. Then, the binary image presents the final results to compare with a standard database. Further,

Peer-reviewed version available at Crystals 2018, 8, 421; doi:10.3390/cryst8110421

the computation adopts the grey comparison of a group of pixels. Thus, the grey threshold is compared with the neighbours in both horizontal and vertical directions. In the history of colour science, several approaches and models have been developed to evaluate colour judgement feasibility and have been applied to analyse colour differences. Among these, in relation to FPDs, the tristimulus colorimeter method is the most popular and measures a diverse colour space through non-contact optical measurements, including colour gamut, colour shift, and chromaticity difference, which was established by the International Commission on Illumination (CIE). Trichromacy can derive non-contact optical measurements by transmitted light spectrometer in the wavelength range of 380 nm to 780 nm. The task utilises the spectral distribution of the transmitted light to determine the chromaticity engaged LED lamp with the whole spectrum. However, if the spectrometer does not limit the visible wavelength, the light source can illuminate the whole optical spectrum from 380 nm to 1700 nm and even beyond. The formulas for the CIE *XYZ* colour space are given below:

$$X = F\int_{380}^{780} T(\lambda)S(\lambda)\,\bar{x}(\lambda)d\lambda \quad (1)$$

$$Y = F\int_{380}^{780} T(\lambda)S(\lambda)\,\bar{y}(\lambda)d\lambda \quad (2)$$

$$Z = F\int_{380}^{780} T(\lambda)S(\lambda)\,\bar{z}(\lambda)d\lambda \quad (3)$$

$$F = \frac{100}{\int_{380}^{780} S(\lambda)\,\bar{y}(\lambda)d\lambda} \quad (4)$$

In the above equations, CIE *XYZ* presents the tristimulus colour value through the spectrometer measurements. Among the various colour systems, the CIE standard takes the spectrum response from the tristimulus values *X*, *Y*, and *Z* with the spectral matching functions *x(λ)*, *y(λ)*, and *z(λ)* to obtain the normalised chromaticity coordinates *x*, *y*, and *z*. By tristimulus values *X*, *Y*, *Z*, the chromaticity coordinates *x*, *y*, and *z* are obtained as shown below [9]:

$$x = \frac{X}{X+Y+Z} \quad (5)$$

$$y = \frac{Y}{X+Y+Z} \quad (6)$$

$$z = \frac{Z}{X+Y+Z} \quad (7)$$

The colour difference ΔE is designed to distinguish perceived colours quantitatively to judge colour deviation [10, 11]. Colour difference is typically expressed in terms of Euclidean distance and is a metric of interest in colour science. Moreover, ΔE is an index of visual perceptibility between the background and foreground, and its threshold is determined through repeated measurements. The colour difference ΔE is treated as the perceptual analogy of colour appearance for human vision. The value ΔE is generally used to classify various visibility levels to reflect the perceivable degree of colour difference by certain criteria [12]. Furthermore, The International Commission on Illumination (CIE) presents the colour distance of the metric ΔE*ab, which occasionally the terminology expresses the ΔE*, dE*, dE, or "Delta E". The perceptual non-uniformities in the CIELAB color space have led to the CIE refining the definition over the years, leading to the superior as recommended by the CIE1994 and CIEDE2000. These non-uniformities are important because the human eye is more sensitive to certain colour than others. A good metric should take this into account in order for the notion of a "just noticeable difference" to have meaning. Otherwise, a certain ΔE that may be insignificant between two colours in one part of the colour space while being significant in some other part. Thus, the JND value between the two colours, that is, how large the ΔE* gap is, just noticed, and there is no final conclusion. Although there is no practical experience to support, the value '1.0' is often mentioned and used as JND. Mahy et al studied and evaluated a JND value of 2.3 ΔE in 1994[13]. However, in the CIELAB colour space that supports the theory, the non-uniformity of perception. In other words, when some colours change, the human eye is very sensitive to them, and some are not clearly distinguished, this theory does not stand too much. As a result, this allowed CIE to use the next few years to fix their definitions and eventually produced a more complete (according to CIE) formula for 1994 and 2000.

Berns[14] proposed the most prevalent methods to classify ΔE_{ab}, which was perceptibility and acceptability. Initially, the perceptibility threshold indicated what magnitude of colour difference was the JND, in which a JND unit that was less than 1 predicted to be imperceptible for viewing side by side[15]. Afterword, the acceptability was classified by three colour difference levels to describe the three vision sections, which were non-perceptibility, hardly perceptible, and easy perceptibility. Furthermore, Perez *et al.* [16] determined the 50:50% perceptibility threshold (PT) and 50:50% acceptability threshold (AT) for computer-simulated samples of human gingiva using CIEDE2000 and CIELAB colour difference formulas. As a result, the PT and AT for CIEDE2000 and 95% confidence intervals were 1.1 and 2.8, respectively. Corresponding CIELAB values were 1.7 and 3.7. Nussbaum [15] proposed that two colour samples be viewed to classify $\Delta E_{ab} < 0.2$ as 'non-visible', ΔE_{ab} between 0.2 and 1.0 as 'very small visual', ΔE_{ab} between 1.0 and 3.0 as 'small', ΔE_{ab} between 3.0 and 6.0 as 'medium', and $\Delta E_{ab} > 6.0$ as 'large'. The JND was a quantitative

index to describe the minimal amount of variation in a stimulus perceived by an observer, whereas it was a statistical indication. In the display industry, the CIE *xyY* standard colour systems usually adopt the spectrum response from the tristimulus values *X*, *Y*, and *Z* that are used to obtain the normalised chromaticity coordinates *x*, *y*, and *z*. Through the transformation of the CIE *xyY* colour coordinates, the coordinates (*a, b*) in the CIELAB uniform colour space are as follows:

$$L = 116\left(Y / Y_n\right)^{1/3} - 16 \tag{8}$$

$$a = 500\left[\left(X / X_n\right)^{1/3} - \left(Y / Y_n\right)^{1/3}\right] \tag{9}$$

$$b = 200\left[\left(Y / Y_n\right)^{1/3} - \left(Z / Z_n\right)^{1/3}\right] \tag{10}$$

The symbols X_n, Y_n, and Z_n express the constant for the daylight source. The equations for colour difference are as follows:

$$\Delta E_{1976} = \sqrt{(\Delta L)^2 + (\Delta a)^2 + (\Delta b)^2} \tag{11}$$

$$\Delta E_{1994} = \sqrt{\left(\frac{\Delta L}{K_L S_L}\right)^2 + \left(\frac{\Delta C}{K_C S_C}\right)^2 + \left(\frac{\Delta H}{K_H S_H}\right)^2} \tag{12}$$

$$\Delta E_{2000} = \sqrt{\left(\frac{\Delta L'}{K_L S_L}\right)^2 + \left(\frac{\Delta C'}{K_C S_C}\right)^2 + \left(\frac{\Delta H'}{K_H S_H}\right)^2 + R_T\left(\frac{\Delta C'}{K_C S_C}\right)\left(\frac{\Delta H'}{K_H S_H}\right)} \tag{13}$$

In the above equations, ΔL, Δa, and Δb are the difference in lightness, redness or greenness, and yellowness or blueness, respectively, between the test and reference specimens. The weighting factor *K* depends on the specific application; S_L, S_C, and S_H are the compensation factors for lightness, chrome, and hue, respectively, while $\Delta L'$, $\Delta C'$, and $\Delta H'$ are the specific lightness, chrome, and hue in ΔE_{2000}. It has been found that the colour space of the colour difference formula of CIELAB is not completely uniform. Figure 3 illuminates the various line-scan CCD by signal line, dual line and TDI, accordingly. It demonstrates the TDI CCD acquiring more image in scanning but the line-scan captures the images only one-line that compare of the TDI CCD at the same time. Moreover, The TDI CCD acquires the image with the pixels in synchronization at the moving objects continuously. Figure 4 presents a schematic of the proposed architecture that detects the spot defects onto the panel and measures the chromaticity of the panel. The panel measurement in conveyor reducing the Tact time is necessary because the factory automation not only saves the operated time but also increases the production. In the moment, while the defect is inspected, the system will send out an alarm message.

Peer-reviewed version available at Crystals 2018, 8, 421; doi:10.3390/cryst8110421

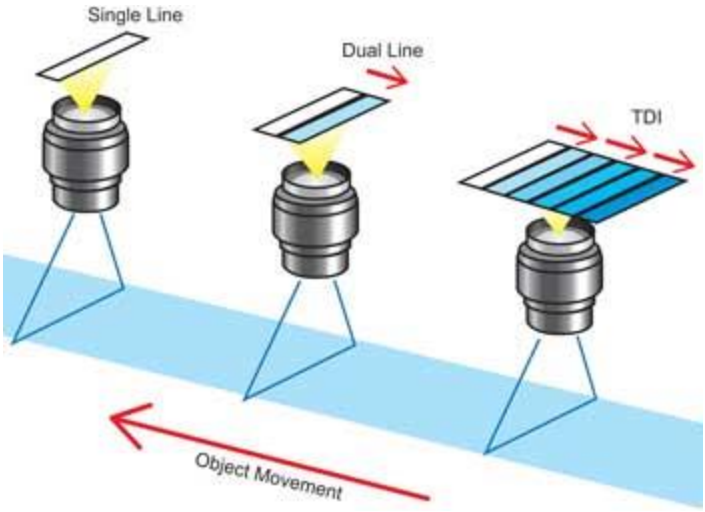

Figure 3 Various line-scan technologies: single-line, dual-line and time delay integration

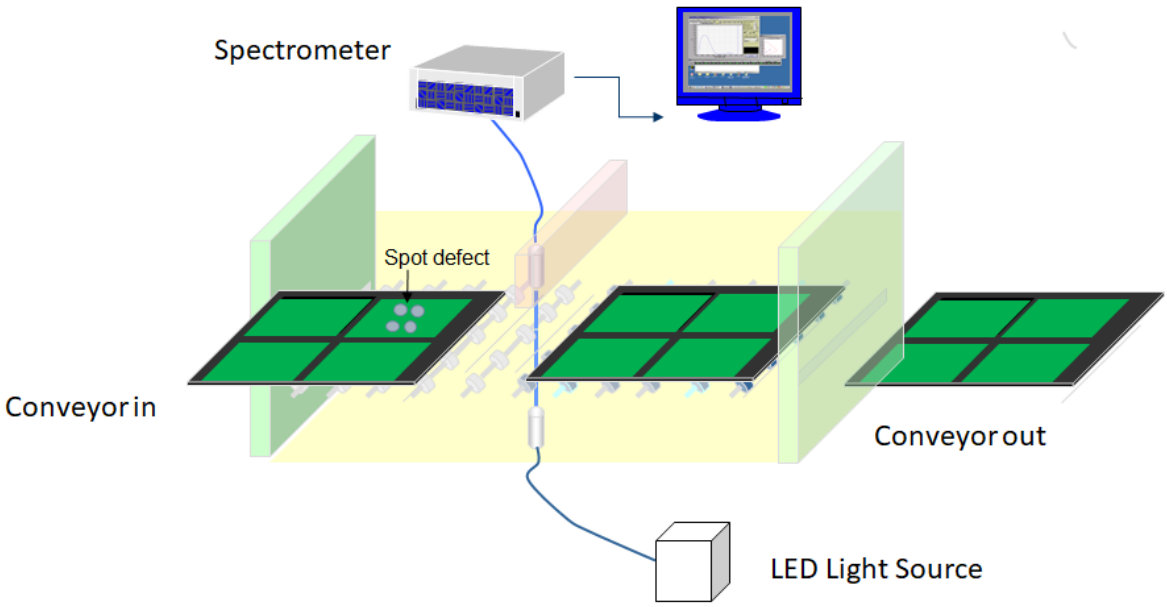

Figure 4 An installation for chromatic measurement by optical device

Experimental Procedure

The task utilizes the automatic optical inspection associated with a chromatic spectrometer to detect non-uniformity defects on the green emission layer of the colour filter 10^{th} generation dimension (2880 mm*3130 mm) in TFT-LCDs that performs the experiment in the class 1000 clean-room at 25^0C. The symmetric architecture uses a photo sensor linking image grabbed card to acquire the information by two-dimensional image. The line-scan TDI-CCD composes the multi array of the pixel sensors, which is applied to the large substrate that moves with constant speed to scan the whole sample. The LED light source emitted to

Peer-reviewed version available at Crystals 2018, 8, 421; doi:10.3390/cryst8110421

the area is capable of detecting the surface for sample. On the other hand, there are four kinds of spot non-uniformity defects on the green layer to be evaluated, labelled as A_1, A_2, B_1, and B_2 in Figure 5 [4]. Both A_1 and A_2 are the samples with artificial defects at 20 mm in diameter, which are a dark region and a low transparency with thick film. By contrast, both B_1 and B_2 are also manmade defects; their diameters are 20 mm a bright region and a high transparency with thin film. Initially, the experimental procedure takes the line scan to obtain the sample imaging for evaluation. The embedded software identifies the grey level variety to judge the threshold. Once the significant defect is over the threshold, the spectrometer moves on the gantry to measure this pseudo defect for chromaticity variety, then automatically presents its colour profiles.

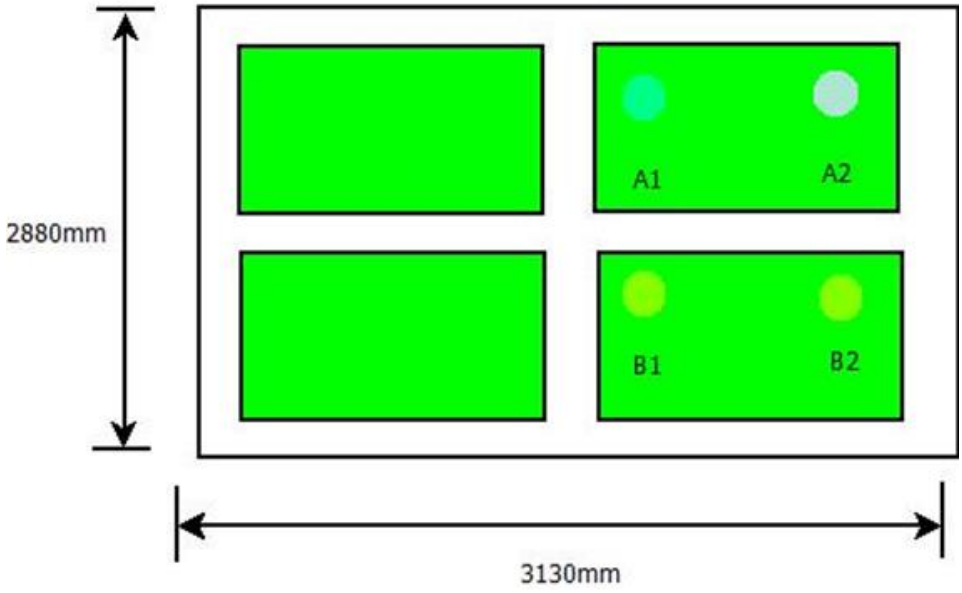

Figure 5 Defect distribution of experimental evaluation in G10th TFT-LCDs[4].

Results and Discussion

Figure 6 shows the different spectral distributions for emissive layers of red, green, blue, and black matrices (BM) through the spectrometer. The spectrum analysis is by 0.8 nm interval wavelength (BTC611E, back-thinned CCD array, working wavelengths from 300 nm to 1050 nm, produced by B&W TEK). Among these photo resists (PRs), the response of green layer reaches 65% for optical response, which is more power intensity than other PRs.

Preprints (www.preprints.org) | NOT PEER-REVIEWED | Posted: 10 September 2018 doi:10.20944/preprints201809.0174.v1

Peer-reviewed version available at Crystals 2018, 8, 421; doi:10.3390/cryst8110421

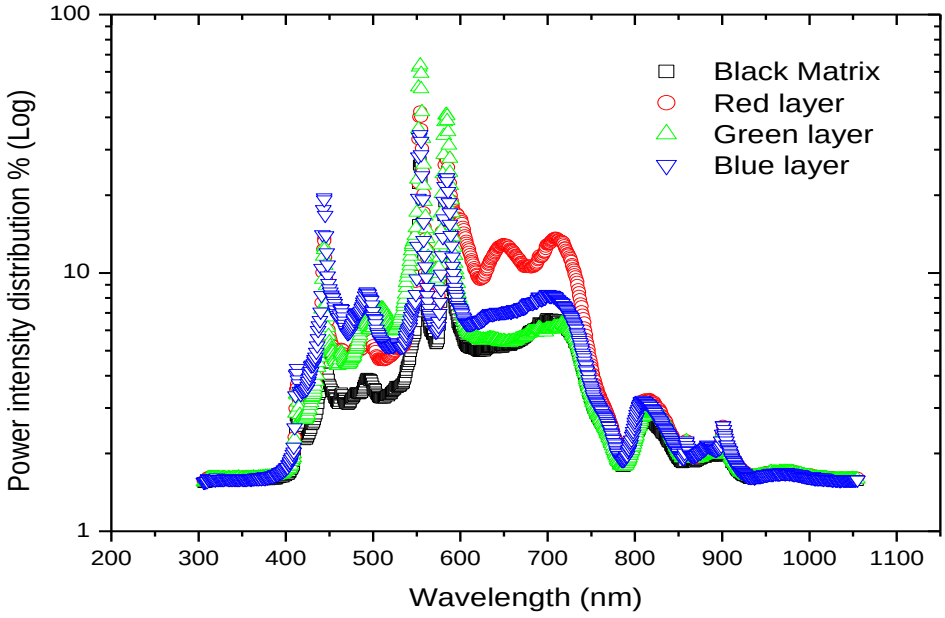

Figure 6 Wavelength distribution for red, green, blue, and black matrices[4].

Figure 7 schemes the CIE *x* profiles across the spot defect to measure its chromaticity at intervals of 1 mm for A_1 and A_2. This task identifies the chromatic tendency versus transparency. As shown, both A_1 and A_2 have a concave tendency with dark region as well as low transparency. Thus, CIE *x* on green emission layer is reversed to the colour system, with the concave tendency in the dark region.

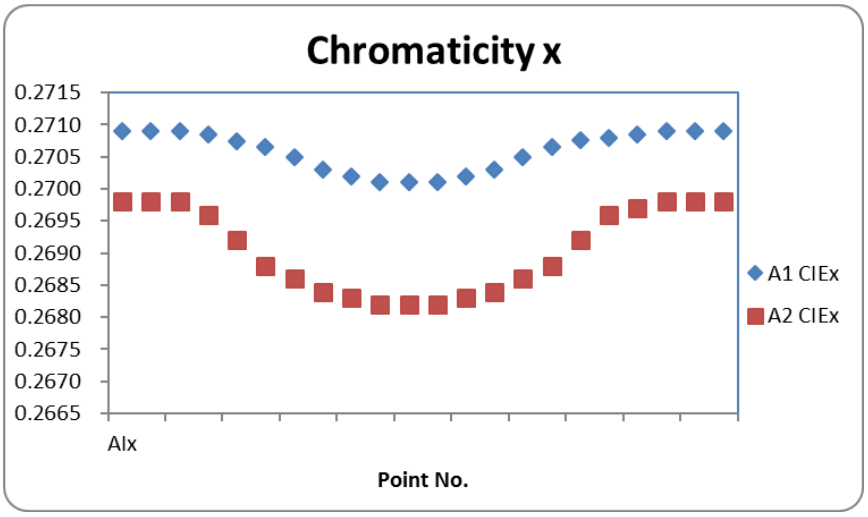

Figure 7 Profile of CIE *x* for A_1 and A_2

Figure 8 shows the CIE *x* profiles across the spot defect to measure its chromaticity at intervals of 1 mm for B_1 and B_2. This task identifies the chromatic tendency versus

Preprints (www.preprints.org) | NOT PEER-REVIEWED | Posted: 10 September 2018 doi:10.20944/preprints201809.0174.v1

Peer-reviewed version available at Crystals 2018, 8, 421; doi:10.3390/cryst8110421

transparency. As shown, both B_1 and B_2 have a convex tendency, which is the bright region and high transparency. Thus, CIE *x* on green emission layer is reversed to the colour system, with the convex tendency in the bright region, and vice versa.

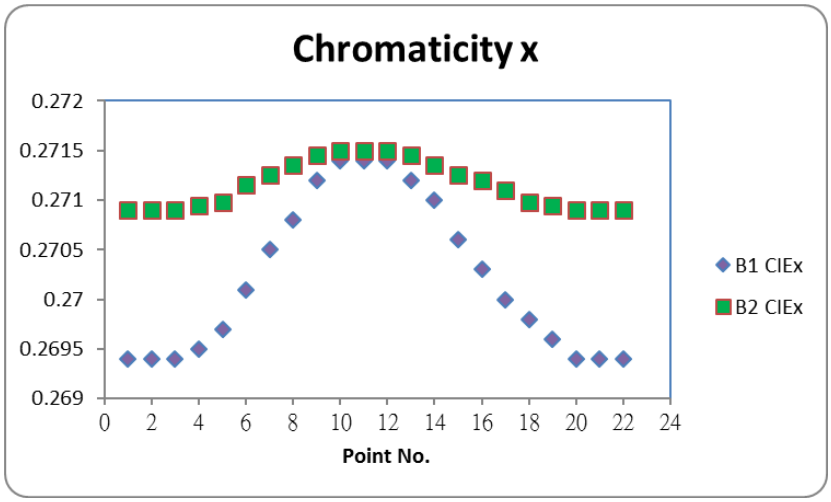

Figure 8 Profile of CIE *x* for B_1 and B_2

Figure 9 is shown the CIE *y* tendency in which the samples of A_1 and A_2 have a convex characteristic, which is the dark region and low transparency. The CIE *y* demonstrates a proportional film thickness; with the larger chromaticity, the thicker film and with the less chromaticity, the thinner film, and vice versa [12]. For the evaluation of colour tendency, the chromaticity of CIE *y* is also used to judge the blue layer film in the flat panel industry [12, 17].

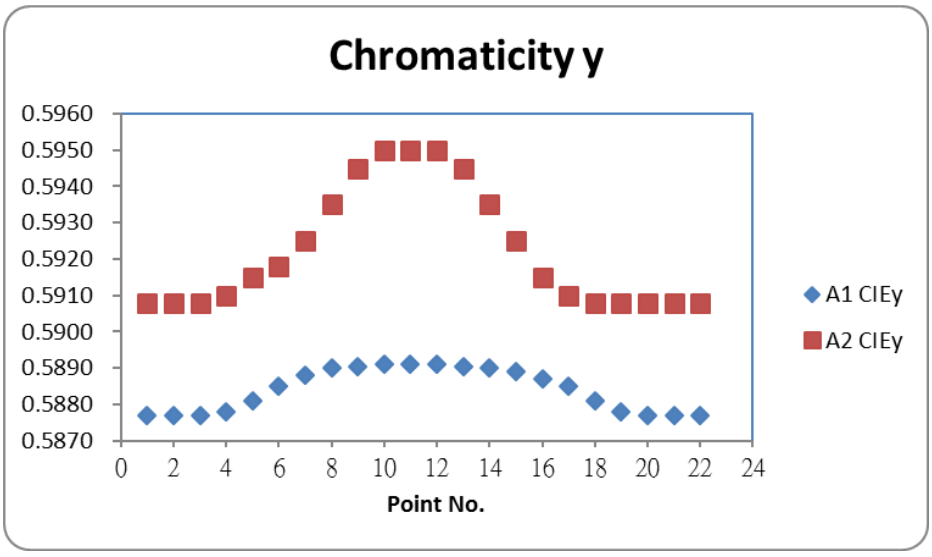

Figure 9 Profile of CIE *y* for A_1 and A_2

Figure 10 is shown the CIE *y* tendency in which the samples of B_1 and B_2 have a concave feature, which is the bright region and high transparency. The CIE *y* demonstrates a

proportional film thickness; with the larger chromaticity, the thicker film and with the less chromaticity, the thinner film, and vice versa.

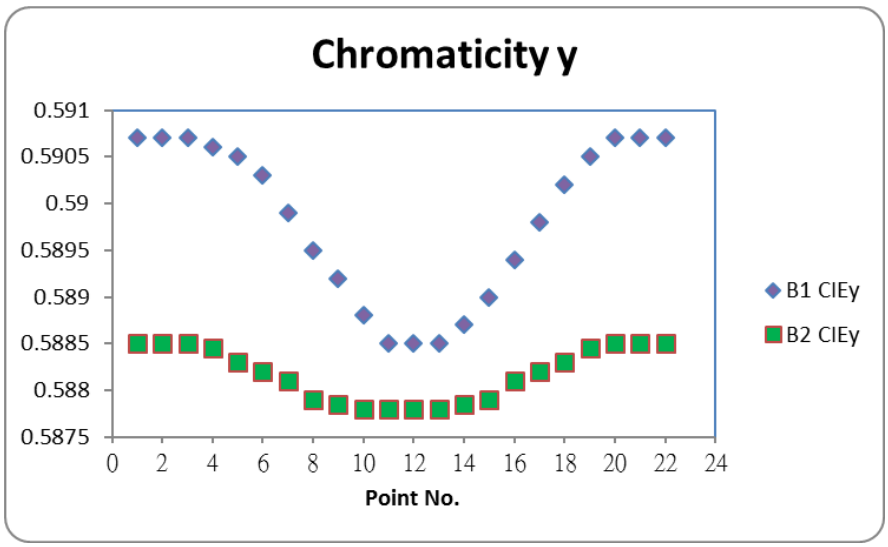

Figure 10 Profile of CIE *y* for B_1 and B_2

Figure 11 exhibits the CIE *Y* to represent various bright regions when the transmitted light passes through the region of the spot non-uniformity. The transmitted light always reverses to thickness, regardless of the transparent material. The thin film has high transparency, while the thick film has low transparency, and vice versa. Thus, both A_1 and A_2 have a concave tendency with thick film, and both B_1 and B_2 are convex profiles with thin film in CIE *Y* as Fig. 12.

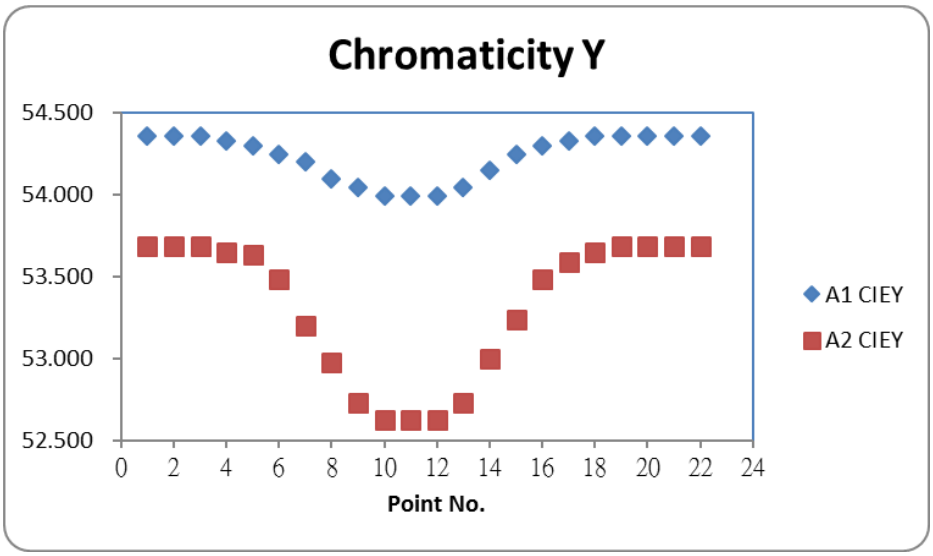

Figure 11 Profile of CIE *Y* for A_1 and A_2

Preprints (www.preprints.org) | NOT PEER-REVIEWED | Posted: 10 September 2018 doi:10.20944/preprints201809.0174.v1

Peer-reviewed version available at Crystals 2018, 8, 421; doi:10.3390/cryst8110421

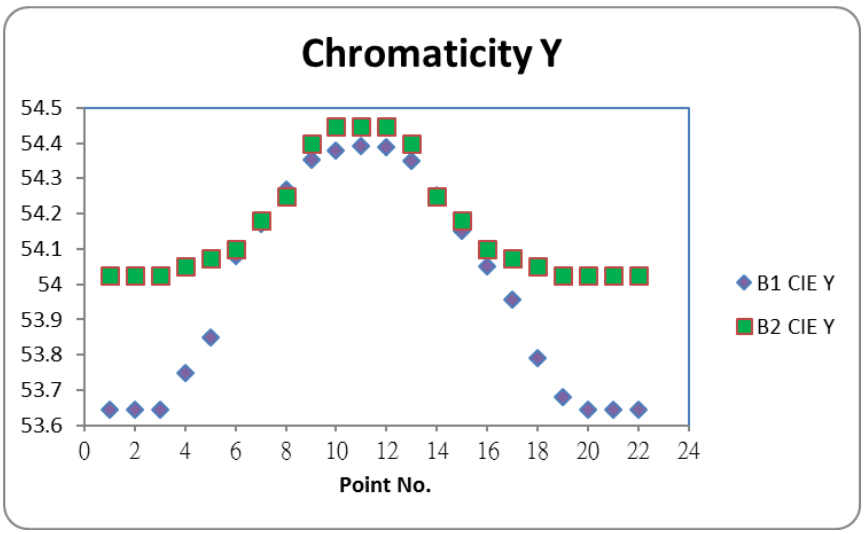

Figure 12 Profile of CIE *Y* for B_1 and B_2

Figure 13 presents the distribution of the colour gamut of the defects, A_1, A_2, B_1 and B_2 based on CIE xyY colour space. The triangle area uses the mathematic vector to be depicted the colour space. However, the imaging quality of colour saturation is very poor due the defects. Assuming the blue and red colour is a chromaticity as equivalent as NTSC standard. Usually, the colour gamut can analyse the colour saturation, vivid, sharp as well as contrast in the fully colour of the display. The task presents these defects with deficient colour saturation to be comparison in the chart. As a result, the defects are more perceptual in the display.

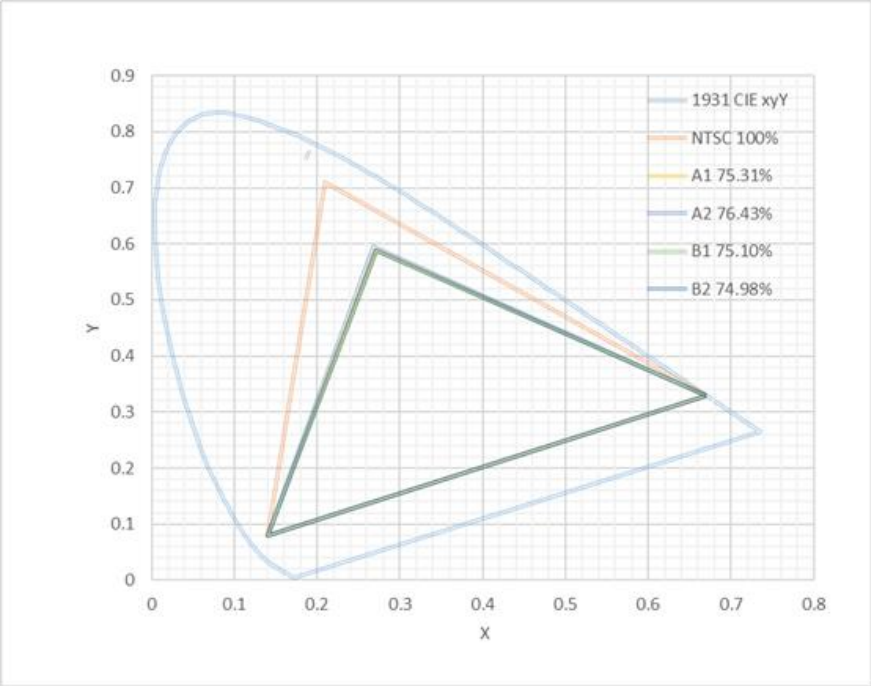

Figure 13 CIExyY colour distribution of A_1, A_2, B_1 and B_2

Figure 14 present the architecture of the calibrated spectrometer linking ^{198}Hg

Peer-reviewed version available at Crystals 2018, 8, 421; doi:10.3390/cryst8110421

discharged lamp, which utilizes the measurement of spectral line to calibrate the spectrometer of spectral line in the visual spectrum [18-20]. This calibrated apparatus adopts the Oriel Instruments, model 6034 pencil lamp. The criterion defines that the shift of the wavelength is small than 1 pixel for spectrometer which 1 pixel calculates based on spectrometer capacity, that is maximum value minus to minimum value then divide to spectrometer resolution. In this task, 1 pixel is at (1050-380)/256=2.6nm. On the other hand, the measurement of the standard deviation is at 0.8nm for the spectrometer.

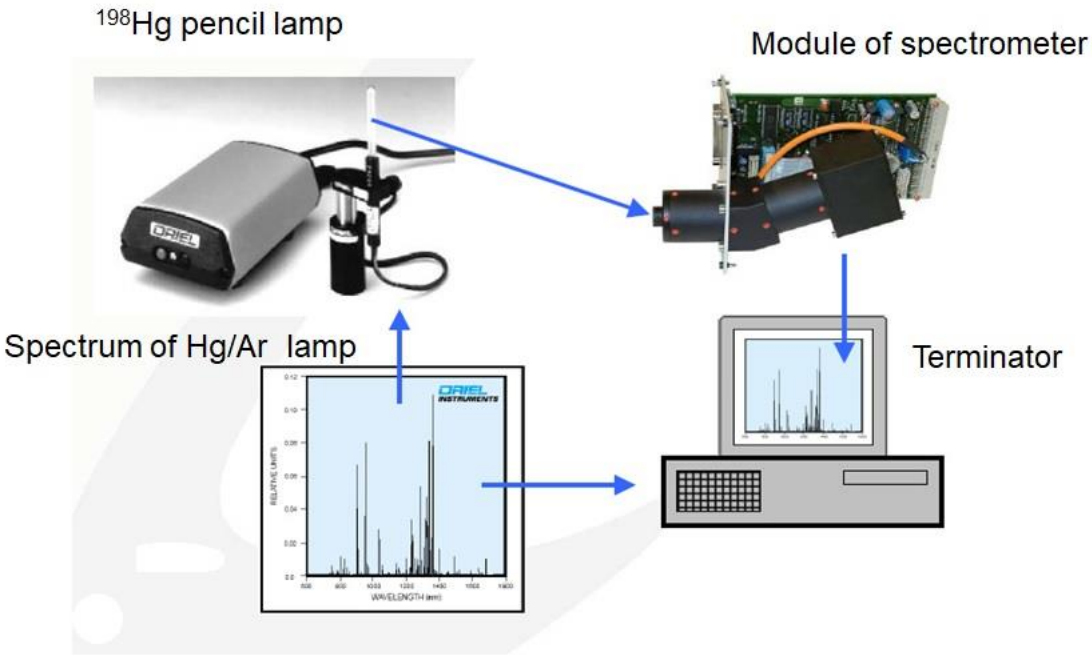

Figure 14 Architecture of 198Hg pencil lamp

Table 1 indicates the various colours in the range for CIE *xyY*, in which CIE *x* is 0.001, 0.004, 0.002, and 0.001 for evaluated samples of A_1, A_2, B_1, and B_2, respectively. In addition, CIE *y* is 0.002, 0.006, 0.003, and 0.002. Moreover, CIE *Y* is 0.5, 1.5, 0.9, and 0.4 for A_1, A_2, B_1, and B_2, accordingly; A_2 is the maximum variation of CIE *Y*. The reading measures ten times of the repeatability is for each samples in the exam.

Table 1 Statistics for colour variation for CIE *xyY*.

Samples	CIE x	CIE y	CIE Y
A_1	0.001	0.002	0.5
A_2	0.004	0.006	1.5
B_1	0.002	0.003	0.9
B_2	0.001	0.002	0.4

Table 2 tabulates the JND statistic according to colour difference referring to the formula

of CIE1976, CIE1994, and CIEDE2000, which presents the visual intensity; except for A_2, these samples indicate imperceptibility by human eyes. The ΔE colour differences of A_2 are 3.3, 1.3, and 1.0 for CIE1976, CIE1994, and CIE2000, accordingly. That is an obvious defect on the task. The optical detected results show that the spot non-uniformity defects can be identified, even if the chromatic difference in CIE *x* and CIE *y* is below 0.001. In contrast, the colour gamut compares to the 100% standard of NTSC that tabulates shown the defects of the A_1, A_2, B_1 and B_2 at 75.31%, 76.43%, 75.10% and 74.98%, respectively. As a result, the defects are shown very poor colour saturation.; however, its colour difference is also the most significant; whereas, high colour difference, low colour gamut. Furthermore, AOI can be detectable for the whole sample but MOI is only perceptible for A_2, whereas the other spot non-uniformity defects are hardly perceptible by human vision.

Table 2 Colour differences base on the formula of 1976, 1994, and 2000, and colour gamut

Samples	$\Delta E1976_{JND2.3}$	$\Delta E1994_{JND1.0}$	$\Delta E2000_{JND1.0}$	CIE xyyY %
A_1	0.9	0.4	0.3	75.31%
A_2	3.3	1.3	1.0	76.43%
B_1	1.8	0.7	0.5	75.10%
B_2	1.1	0.4	0.3	74.98%

In the end, Table 3 tabulates the ^{198}Hg discharge lamp with spectral lines to identify the standard deviation of spectral measurement.

Table 3 Standard deviation of the spectrometer by calibrated ^{198}Hg discharged lamp

Measured (nm)	Lamp (nm)	Difference (nm)
404.077	404.656	-0.579
434.232	435.835	-1.603
545.529	546.074	-0.545
577.305	576.959	0.346
Standard deviation		0.797

Conclusions

An automatic optical method using a line-scan mode TDI-CCD engaged transmitted spectrometer to detect non-uniformity of the green emission layer for ultra-high resolution of TFT-LCDs is presented. The evidence shows a significant breakthrough to identify spot non-uniformity related to chromatic tendency, and even JND is lower than the perceptibility threshold. Moreover, the CIE *x* on the green emission layer is reversed to the colour system (i.e., with the concave tendency, the dark region and with the convex tendency, the bright region, and vice versa). The CIE *y* demonstrates a proportional film thickness, i.e., with the

larger chromaticity, the thicker film and with the less chromaticity, the thinner the film, and vice versa. On the other hand, for CIE *Y*, both A_1 and A_2 have a concave tendency with thick film, and both B_1 and B_2 have a convex tendency with thin film. The AOI is able to detect the capacity which reaches the intensity of colour difference at 0.3 based on theΔE_{2000}, which is more sensitive than that of the JND. As a result, AOI may detectable for the whole sample but MOI has a perceptible for A_2 in the study, whereas the additional spot non-uniformity defects are hardly perceptible by MOI. This proposed method has an accurate visual system to quantify the defects be substituting for MOI in the display world.

Reference

1. Liu S., Wang D., Yang Z. K., Feng X., Sun X., Qiu Y., et al. Key technology trends analysis of TFT-LCD. Chinese Journal of Liquid Crystals and Displays **2018**, 33, 457-463
2. Li X. H., Bao J. P., Xu B., Fan H. Y. Improvement research of TFT-LCD module black uniformity. Chinese Journal of Liquid Crystals and Displays **2018**, 33, 271-276
3. Hammer M., Hinnen K. J. G. Local Luminance Boosting of an RGBW LCD. Journal of Display Technology **2014**, 10, 33-42
4. Tzu F. M., Chou J. H. Non-uniformity evaluation of flat panel display by automatic optical detection. 2016 11th International Microsystems, Packaging, Assembly and Circuits Technology Conference (IMPACT) **2016**, 168-171
5. Kwon K. J., Kim M. B., Heo C., Kim S. G., Baek J. S., Kim Y. H. Wide color gamut and high dynamic range displays using RGBW LCDs. Displays **2015**, 40, 9-16
6. Kim D. U., Kim J. S., Choi B. D. A Low-Power Data Driving Method With Enhanced Charge Sharing Technique for Large-Screen LCD TVs. Journal of Display Technology **2015**, 11, 346-352
7. L. Bergman J. L. M. Handbook of Luminescent Semiconductor Materials. CRC Press **2016**, 268~270
8. Tzu F. M., Chou J. H. Spot Mura evaluation in TFT-LCDs using automatic optical inspection. 2010 5th International Microsystems Packaging Assembly and Circuits Technology Conference **2010**, 1-4
9. Gomez-Polo C., Munoz M. P., Lunego M. C. L., Vicente P., Galindo P., Casado A. M. M. Comparison of the CIELab and CIEDE2000 color difference formulas. Journal of Prosthetic Dentistry **2016**, 115, 65-70
10. Strocka D. Color difference formulas and visual acceptability. Applied Optics **1971**, 10, 1308-1313
11. Gomez-Polo C., Munoz M. P., Luengo M. C. L., Vicente P., Galindo P., Casado A. M. M. Comparison of two color-difference formulas using the Bland-Altman approach based on natural tooth color space. Journal of Prosthetic Dentistry **2016**, 115, 482-488
12. Tzu F. M., Chou J. H. Slit-Mura Detection through Non-contact Optical Measurements

of In-Line Spectrometer for TFT-LCDs. Ieice Transactions on Electronics **2009**, E92C, 364-369

13. Mahny M., Vaneycken L., Oosterlinck A. Evaluation of uniform color spaces developed after adoption of CIELAB and CIELUV. Color Research and Application **1994**, 19, 105-121
14. R. B. Billmeyer and Saltzman's principles of color technology. Wiley New York **2000**,
15. Nussbaum P. Colour Measurement and Print Quality Assessment in a Colour Managed Printing Workflow. Doctoral Dissertation, The Norwegian Color Research Laboratory Faculty of Computer Science and Media Technology **2011**, 264-284
16. Perez M. M., Ghinea R., Herrera L. J., Carrillo F., Ionescu A. M., Paravina R. D. Color difference thresholds for computer-simulated human Gingiva. Journal of Esthetic and Restorative Dentistry **2018**, 30, E24-E30
17. Lee J. Y., Yoo S. I. Automatic detection of region-mura defect in TFT-LCD. Ieice Transactions on Information and Systems **2004**, E87D, 2371-2378
18. Martinsen P., Jordan B., McGlone A., Gaastra P., Laurie T. Accurate and precise wavelength calibration for wide bandwidth array spectrometers. Applied Spectroscopy **2008**, 62, 1008-1012
19. Veza D., Salit M. L., Sansonetti C. J., Travis J. C. Wave numbers and Ar pressure-induced shifts of Hg-198 atomic lines measured by Fourier transform spectroscopy. Journal of Physics B-Atomic Molecular and Optical Physics **2005**, 38, 3739-3753
20. Sansonetti C. J., Salit M. L., Reader J. Wavelengths of spectral lines in mercury pencil lamps. Applied Optics **1996**, 35, 74-77